HEALTH AND MEDICINE

Transplanted organoids empower human preclinical assessment of drug candidate for the clinic

Amy D. Westerling-Bui[1]*, Eva Maria Fast[1], Thomas W. Soare[1]†, Srinivasan Venkatachalan[1]‡, Michael DeRan[2], Alyssa B. Fanelli[1], Sergii Kyrychenko[1]§, Hien Hoang[1]‖, Grinal M. Corriea[1]¶, Wei Zhang[1]#, Maolin Yu[1], Matthew Daniels[1]††, Goran Malojcic[1]‡‡, Xin-Ru Pan-Zhou[1], Mark W. Ledeboer[1]§§, Jean-Christophe Harmange[1]‖‖, Maheswarareddy Emani[3]¶¶, Thomas T. Tibbitts[1]##, John F. Reilly[1]***, Peter Mundel[1]*†††§§§**

Pharmacodynamic (PD) studies are an essential component of preclinical drug discovery. Current approaches for PD studies, including the analysis of novel kidney disease targeting therapeutic agents, are limited to animal models with unclear translatability to the human condition. To address this challenge, we developed a novel approach for PD studies using transplanted, perfused human kidney organoids. We performed pharmacokinetic (PK) studies with GFB-887, an investigational new drug now in phase 2 trials. Orally dosed GFB-887 to athymic rats that had undergone organoid transplantation resulted in measurable drug exposure in transplanted organoids. We established the efficacy of orally dosed GFB-887 in PD studies, where quantitative analysis showed significant protection of kidney filter cells in human organoids and endogenous rat host kidneys. This widely applicable approach demonstrates feasibility of using transplanted human organoids in preclinical PD studies with an investigational new drug, empowering organoids to revolutionize drug discovery.

INTRODUCTION

Despite exciting advances to address unmet medical needs, there remains a substantial imperative to discover new treatments for many diseases. However, drug development has been hampered by the limited predictive power and translatability of pharmacodynamic (PD) studies in animal models to the human condition. To overcome this critical problem, we need a scalable approach for preclinical PD studies that includes a human component. The problem is particularly urgent for kidney diseases, where progress with drug development has been slow (*1*). One in nine people worldwide suffer from chronic kidney disease (CKD), making it a global epidemic affecting more than 850 million people (*2*).

A new and exciting opportunity for human preclinical drug evaluation is induced pluripotent stem cell (iPSC)–derived organoids (*3*), including kidney organoids (*4*–*14*). While organoid systems can faithfully model three-dimensional human tissues, their applicability to preclinical PD studies to bolster confidence in an investigational new drug before it enters phase 1/2 clinical studies has remained aspirational. To date, organoids have not been used to capture what an intact organism (e.g., mouse, rat, dog, or human) does to a drug [pharmacokinetic (PK) evaluation], nor how a drug perturbs its target in an intact organism (PD evaluation).

Here, we describe a scalable approach for human preclinical PD assessment of drugs targeting podocytes, cells essential to the kidney filter barrier (*15*). Podocyte damage leads to many kidney diseases, including focal segmental glomerulosclerosis (FSGS), the most common histologic diagnosis associated with CKD worldwide (*16*). We successfully performed PD studies with GFB-887, a novel investigational small-molecule transient receptor potential canonical 5 (TRPC5) inhibitor, in human kidney organoids transplanted into rats. Orally administered GFB-887 reached human podocytes in transplanted organoids at a therapeutically meaningful concentration (PK study) and engaged its target (TRPC5) to confer therapeutic benefit (PD study). We thus demonstrate how human organoids can be used for preclinical PD studies, thereby overcoming the limitations of PD studies in traditional animal models.

RESULTS

Generation of kidney organoids suitable for PD studies

To generate high-quality human kidney organoids suitable for PD studies at scale, we made several key modifications to published protocols (*5*, *8*, *13*, *14*, *17*, *18*) (Material and Methods and fig. S1), including (i) optimized iPSC seeding on T75 flasks, (ii) cell quantifying in suspension, (iii) reproducibility monitoring of organoid differentiation, (iv) optimized timing and density for Transwell dish seeding, and (v) refined dissociation for increased cell viability. These key modifications allowed us to routinely produce 500 organoids per batch with increased reproducibility in a short time frame.

To determine whether the organoids generated with the modified protocol were appropriately differentiating in a scalable, reproducible manner, we assessed their composition by fluorescence-activated

[1]Goldfinch Bio Inc., Cambridge, MA 02142, USA. [2]Diamond Age Data Science, Somerville, MA 02143, USA. [3]Broad Institute of MIT and Harvard, Cambridge, MA 02142, USA.
*Corresponding author. Email: amydbui@gmail.com (A.D.W.-B.); petermundel@icloud.com (P.M.)
†Present address: Insitro, South San Francisco, CA 94080, USA.
‡Present address: Walden Biosciences, Cambridge, MA 02139, USA.
§Present address: Prime Medicine, Cambridge, MA 02139, USA.
‖Present address: Editas Medicine, Cambridge, MA 02141, USA.
¶Present address: Tango Therapeutics, Cambridge, MA, 02142, USA.
#Present address: Bristol-Myers Squibb, San Diego, CA 92121, USA.
**Present address: Nirogy Therapeutics, Framingham, MA 01702, USA.
††Present address: Accent Therapeutics, Cambridge, MA, 02142, USA.
‡‡Present address: Novartis, 4057 Basel, Switzerland.
§§Present address: Expansion Therapeutics, Jupiter, FL 33458, USA.
‖‖Present address: Triana Biomedicines, Waltham, MA 02451, USA.
¶¶Present address: Genentech, South San Francisco, CA 94080, USA.
##Present address: Dogodan Therapeutics, Westford, MA 01886, USA.
***Present address: Nereid Therapeutics, Boston, MA 02210, USA.
†††Present address: Atlas Venture, Cambridge, MA, 02139, USA.
§§§Lead contact.

cell sorting (FACS) flow cytometry (fig. S2) and comprehensive single-cell RNA sequencing (scRNA-seq) profiling. We clustered cells with similar transcriptional profiles and labeled these clusters based on expression of previously described marker genes (table S1). Since the time period between day 7 (D7) and D15 in vitro is critical for kidney organoid differentiation and variability (*8*), we profiled organoids at D0 (iPSC state) and on D7, D10, D12, and D14. We also profiled late-stage organoids on D24, D26, and D28. In total, we profiled 204,748 single cells from 24 organoids across all time points (fig. S1, A and B). iPSCs on D0 maintained a high level of pluripotency (figs. S1, B to D, and S3A) and matched published transcriptomic signatures (*8*). On D7, developing organoids expressed appropriate markers of mesodermal differentiation with actively proliferating cells (*19*) and little variability between replicates (figs. S1B and S3B). By D10, nephron progenitor cells appeared, which represented most of the cells through D14 (figs. S1B and S3, C to E). Of particular interest to our work are podocytes, cells critical for maintaining the kidney filter barrier (*15*), and tubular epithelial cells, and we thus focused on signature genes for these cell types (figs. S1, B to D, and S3, F to H). Marked differences in cell type proportions were observed across time points [mean Jensen-Shannon divergence (JSD) = 0.22, SD = 0.27; figs. S1B and S4A], but differences among replicates were small (mean JSD = 0.0015, SD = 0.0016; figs. S1B and S4B). Thus, most of the variations, which became apparent at D10, were due to differences between stages of organoid differentiation and not due to variability between replicates of the same stage. From these results, we concluded that the differentiation of kidney organoids using our novel, scalable protocol is highly reproducible.

We went on to validate the scRNA-seq data using a novel NanoString gene expression panel for rigorous and rapid organoid quality control (QC) (figs. S5 and S6). The NanoString panel made it feasible to decide as early as D7 whether the quality of organoid batch was sufficient to continue differentiation, or whether the quality was poor, necessitating that we discard the batch and start a new batch (figs. S5 and S6). We also conducted a time course gene expression analysis for the pre- and posttransplantation periods (fig. S7). The time course analysis allowed us to monitor the quality and reproducibility of individual transplanted organoids, which is paramount in drug discovery.

Transplantation induces organoid perfusion sufficient for oral drug delivery

PD studies require an intact organism with a circulatory system and the capacity to metabolize candidate drugs under evaluation, and organoids grown in vitro are, by definition, not perfused by a systemic circulation. Therefore, we sought to develop a method for measuring PD for a given drug in a human organoid transplanted into and perfused by the circulation of a host species. Vascularization of transplanted kidney organoids has been published (*7*–*9*, *20*), but it remains unclear whether transplanted organoids are also sufficiently perfused so that a drug can reach the organoids at concentrations high enough to be efficacious in PD studies. To answer this key question, we grew organoids in vitro for 10, 12, or 14 days before inserting them under the kidney capsule of athymic rats (Fig. 1A). We chose rats as host because rats are most commonly used for PD studies. We further grew the organoids for 2 or 4 weeks in vivo before harvesting them for scRNA-seq, NanoString, and image analysis (Fig. 1A and fig. S7). We profiled 143,475 cells from 18 transplanted organoids from three staggered batches by scRNA-seq. The generation of staggered batches allowed us to transplant three independent sets of organoids on the same day. Compared to in vitro maturation, the fraction of differentiated podocytes and tubular epithelial cells increased with in vivo maturation (Fig. 1B). A longer period of in vivo maturation resulted in a greater proportion of differentiated podocytes (0.097 versus 0.066, $P = 0.0035$; Fig. 1C) and proximal tubular cells (0.21 versus 0.11, $P = 0.0032$; Fig. 1C). There were fewer distal tubular cells at 4 weeks ($P = 1.4 \times 10^{-12}$; Fig. 1C), an effect driven by the lack of distal tubule cells at the D10–4-week time point. When comparing 2 weeks versus 4 weeks of in vivo maturation, we noted a trend toward more off-target cell types in the 4-week transplanted organoids (0.063 versus 0.022, $P = 0.15$; Fig. 1C). Differences between time points were observed between transplantation days (mean JSD = 0.099, SD = 0.050; Fig. 1C and fig. S8A) and between weeks of in vivo maturation (mean JSD = 0.081, SD = 0.062; Fig. 1D and fig. S8B). To understand the differentiation state of cells within clusters, we performed trajectory analysis of podocytes and nephron progenitor cells from our organoids with fetal and adult human kidney (*21*–*23*) as an end point. Comparing mean pseudotime of different transplantation time points to human fetal and adult podocytes allowed us to evaluate how transcriptionally similar our organoid podocytes are to the human gold standard. Our trajectory analysis showed that human samples are associated with higher mean pseudotime (Fig. 1D). We thus inferred that organoid-derived podocytes with higher mean pseudotime are more similar to human kidney–derived cells. Podocytes from organoids harvested 4 weeks after transplantation had a significantly increased mean pseudotime (mean pseudotime = 18, SD = 5.6) compared to podocytes 2 weeks after transplantation for all time points (mean pseudotime = 16, SD = 6.4, $P = 1.5 \times 10^{-30}$, *t* test two-sided; Fig. 1D and fig. S9, A to D). Furthermore, pseudotime of organoids was highest when transplanted at D14 (mean pseudotime = 21, SD = 3.7, Tukey $P < 10^{-7}$) when compared within a transplanted group (2 or 4 weeks). Within the distal tubular cell cluster, we observed a small population of cells expressing significantly greater levels of *AQP2*, *CALB1*, *CDH1*, and *KRT8*, markers of collecting duct cells (fig. S10, A to C) (*8*). A trajectory analysis using distal tubular and collecting duct cells from human samples revealed no clear transition between these two cell types (fig. S10, D to F), consistent with previous findings (*24*), indicating a different developmental origin of the collecting duct and the remainder of the kidney. Our data therefore indicate that using our protocol, in vivo maturation only promotes further differentiation of cell fates that already exist before transplantation and does not give rise to the new cell fates. In keeping with previous studies (*7*–*9*, *20*), the transplanted organoids underwent successful vascularization by the host, as indicated by the predominant presence of rat endothelial cell antigen 1 (RECA-1)–expressing rat endothelial cells in organoid tissue (Fig. 1E and fig. S11A). We also detected CD31/platelet and endothelial cell adhesion molecule 1 (PECAM1)-expressing human endothelial cells in organoid tissue (Fig. 1F and fig. S11A). The up-regulation of CD31/PECAM1 expression in transplanted organoids was verified by NanoString analysis, and the highest levels of CD31/PECAM1 mRNA expression were found in D14 organoids grown in vivo for 4 weeks (fig. S11B). We also confirmed *AQP2* mRNA up-regulation by NanoString analysis (fig. S11C). Together, transplantation of D14 organoids and further in vivo growth for 4 weeks were best for organoid vascularization and podocyte maturation.

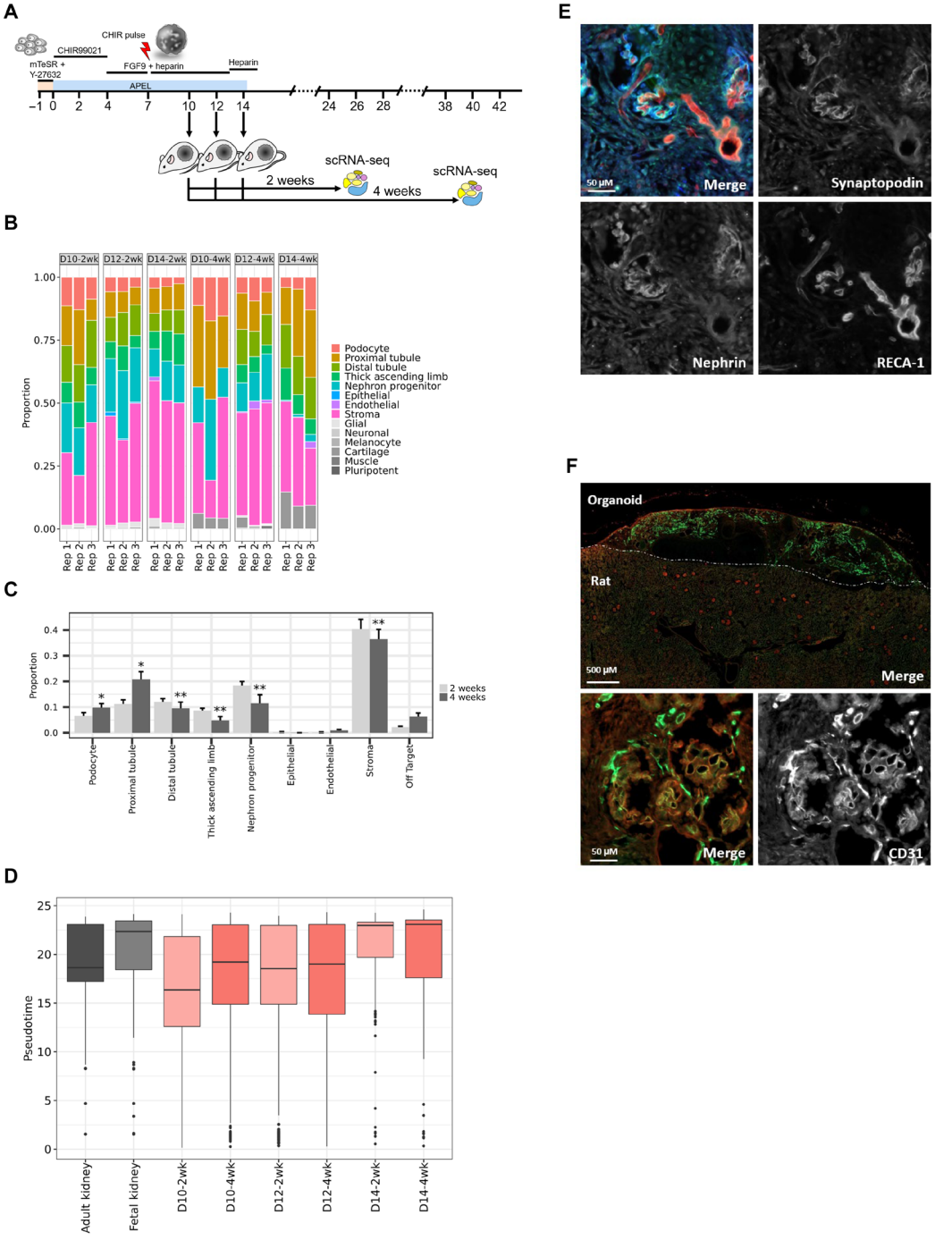

Fig. 1. Transplantation of human kidney organoids in rats promotes vascularization by the rat host systemic circulation. (**A**) Schematic of organoid protocol with transplantation and scRNA-seq time points. (**B**) Stacked bar graph showing cell type proportions of in vivo maturation across six time points (three replicate organoids per time point, 143,475 cells). All replicates for each time point are biological replicates of a single differentiation. The replicates show an increase in podocytes, tubular cells, endothelial cells, and off-target cell types after a prolonged in vivo maturation period. (**C**) Averaged cell type proportions after 2 weeks (light gray) and 4 weeks (dark gray) of in vivo maturation. Differences between cell type proportions tested with Dirichlet regression with significantly different comparisons are marked with one asterisk ($P < 0.05$) or two asterisks ($P < 0.001$). Error bars represent +SEM. (**D**) Boxplots [representing interquartile range (IQR) and median and with whiskers extending to ±1.5× IQR] of pseudotime, a measure of maturation inferred by a trajectory analysis, for podocytes from human samples (gray, 563 cells) and transplanted organoids (red, 10,753 cells). Podocytes from organoids harvested 4 weeks posttransplant had significantly increased pseudotime compared to podocytes from 2 weeks posttransplant organoids for all time points ($P = 1.5 \times 10^{-30}$). (**E**) High-power view showing RECA-1–expressing rat endothelium–derived vascularization of a human organoid glomerulus. Red, RECA-1; green, synaptopodin; blue, nephrin. (**F**) Transplanted organoids develop a vascular network containing CD31/PECAM1-expressing human endothelial cells (top). A higher-magnification image shows CD31/PECAM1-positive human endothelial cells invaginating into a human organoid glomerulus (bottom). Red, RECA-1; green, CD31/PECAM1.

Evaluation of drugs on organoids grown at scale

We next tested the performance of in vitro grown organoids in a head-to-head comparison between the calcineurin inhibitor cyclosporine A (CsA), which is clinically used to treat patients with kidney diseases (*25*), and GFB-887, one of several novel small-molecule inhibitors of TRPC5 channels (*26*). Whole-cell patch clamp electrophysiology in human embryonic kidney (HEK) 293 cells expressing human TRPC5 showed GFB-887–mediated inhibition of TRPC5 current (Fig. 2A) The previously described TRPC5 inhibitor tool compound ML204 (*27*) served as positive control. The median inhibitory concentration of GFB-887 was 0.037 μM (Fig. 2B). By scRNA-seq, we detected a few cells in kidney organoids that expressed *TRPC5* mRNA. Before embarking on functional studies, we confirmed the expression of *TRPC5* in the organoids using the more sensitive NanoString approach. We detected a time-dependent increased expression of *TRPC5* mRNA expression during organoid differentiation with highest *TRPC5* mRNA levels detectable in D40 to D45 organoids (Fig. 2C). The presence of TRPC5 protein in the organoids was further confirmed by double-labeling immunofluorescence microscopy with the podocyte differentiation marker synaptopodin (Fig. 2D and fig. S12) (*28*, *29*).

FSGS is a disorder of podocytes with high likelihood of progression to kidney failure (*15*, *16*, *30*). In animal models of FSGS, inhibition of TRPC5 channels with tool compounds protects against Rac1-driven proteinuria and podocyte loss (*26*, *31*). Here, we chose the protamine sulfate (PS) model of reversible podocyte injury because (i) it has been widely used in rats (*32*, *33*), (ii) PS activates TRPC5 channels (*34*), and (iii) TRPC5 gene deletion or inhibition with a TRPC5 inhibitor tool compound protects against PS-induced podocyte injury (*34*). We compared the protective effects of CsA and GFB-887 on PS-induced, TRPC5-calcineurin-synaptopodin-Rac1 dysregulated podocyte actin dynamics (*27*, *34*–*37*). The regulation of synaptopodin protein abundance is a key PD marker of podocyte dysfunction and injury in FSGS. This has been previously established by revealing that the antiproteinuric effect of CsA, a drug used to treat patients with FSGS, preserves the expression and function of synaptopodin in podocytes (*25*, *35*, *36*). The relevance of synaptopodin for proteinuria and FSGS (*36*) (and thus the validity of synaptopodin as a PD marker and PS-induced actin cytoskeleton rearrangement as an acute injury model for podocyte injury in FSGS) has been further validated in a recent study (*38*). Similar to podocytes in vitro (*34*, *35*), PS induced Rac1-driven actin aggregation, resulting in increased phalloidin labeling in organoid podocytes. Both CsA and GFB-887 protected from PS-driven actin aggregation (Fig. 2E). We quantified the changes in phalloidin labeling (Fig. 2E, blue ring), and, in keeping with the observation that TRPC5 is the ion channel required for calcineurin activation in podocytes (*27*), we found comparable protection by CsA and GFB-887 (Fig. 2F). Since there was no additive effect, we concluded that both compounds block the activation of calcineurin (Fig. 2G).

PD studies in transplanted kidney organoids bolster confidence in GFB-887, an investigational new drug

Having established the in vitro efficacy of GFB-887 in organoids produced by our scalable, quality-controlled protocol, we were poised to conduct the long-sought PD studies with transplanted human organoids. We used rats carrying transplanted kidney organoids to evaluate the effect of GFB-887 on human podocyte injury in vivo. We found that oral dosing of GFB-887 (10 mg/kg) to athymic rats with transplanted D14 organoids for 2 or 4 weeks resulted in measurable drug exposure in rat plasma and rat kidneys and in the transplanted human organoids (PK study; Fig. 3A). Specifically, we quantified drug exposure in human organoids compared to rat plasma and rat kidney tissue and found that GFB-887 orally dosed or three consecutive days before sample collection resulted in equivalent drug exposure in human organoids compared to rat plasma (Fig. 3A). Quantitative whole-body autoradiography showed GFB-887 accumulation in several tissues including the liver, adrenal gland, pancreas, and kidney. Tissue accumulation is a normal phenomenon for small-molecule therapies, which commonly distribute differentially to tissues at higher levels than plasma. For GFB-887, kidney concentrations were typically two- to threefold higher than plasma concentrations (Fig. 3A).

Last, we used rats carrying transplanted D14 organoids for 4 weeks, which develop podocytes that are transcriptionally most similar to human podocytes (Figs. 1B and 3, A to D) to assess PS-induced podocyte injury in the organoids in comparison with endogenous rat kidneys. The transmission electron microscopic validation of the link between PS-induced TRPC5 activation, degradation of synaptopodin, and podocyte foot process effacement, the hallmark of PS-induced podocyte injury (*32*, *33*), has been published before (*34*). Historically, the readout of PS studies had been transmission electron microscopy analysis of kidney tissue (*32*–*34*), which is labor intensive and time consuming and thus not feasible in a drug discovery setting. Therefore, we developed a novel high-throughput approach for the quantification of PS-induced loss of synaptopodin protein abundance (*34*–*36*) that combines fluorescence and super-resolution microscopy (*39*). This novel approach, described in detail in Materials and Methods, takes advantage of the mechanistic link between PS-induced podocyte foot process effacement, activation of TRPC5, and loss of synaptopodin protein abundance (*34*, *37*) as a PD readout of TRPC5 target engagement. We found that PS caused a marked reduction in synaptopodin protein abundance in rat kidney and human organoids (Fig. 3B). The quantitative analysis showed that either coperfusion of GFB-887 (3 μM) with PS or oral dosing of GFB-887 (10 mg/kg) before PS perfusion preserved the abundance of synaptopodin in organoids (PD study; Fig. 3C). Comparable preservation of synaptopodin abundance was noted in podocytes of host rat kidneys (Fig. 3D). Collectively, these data show that the inhibition of TRPC5 channels by GFB-887 effectively protects podocytes not only in rat kidneys but also in transplanted human kidney organoids, bolstering our confidence in the potential therapeutic efficacy of this investigational new drug in patients.

DISCUSSION

In this study, we pioneered a novel approach for in vivo PD studies using transplanted human kidney organoids. In a novel, rigorously quality-controlled system, we established preclinical human efficacy for GFB-887, an investigational new drug now being tested in the clinic (NCT04387448).

This preclinical study with transplanted human organoids has led to several important insights. First, before embarking on PD studies, we established the optimal time frame for organoid transplantation to achieve a high degree of organoid maturation, vascularization, and perfusion. These insights ensured that the transplanted organoids developed a vasculature sufficiently perfused to allow the delivery of a drug to the organoids at concentrations high enough

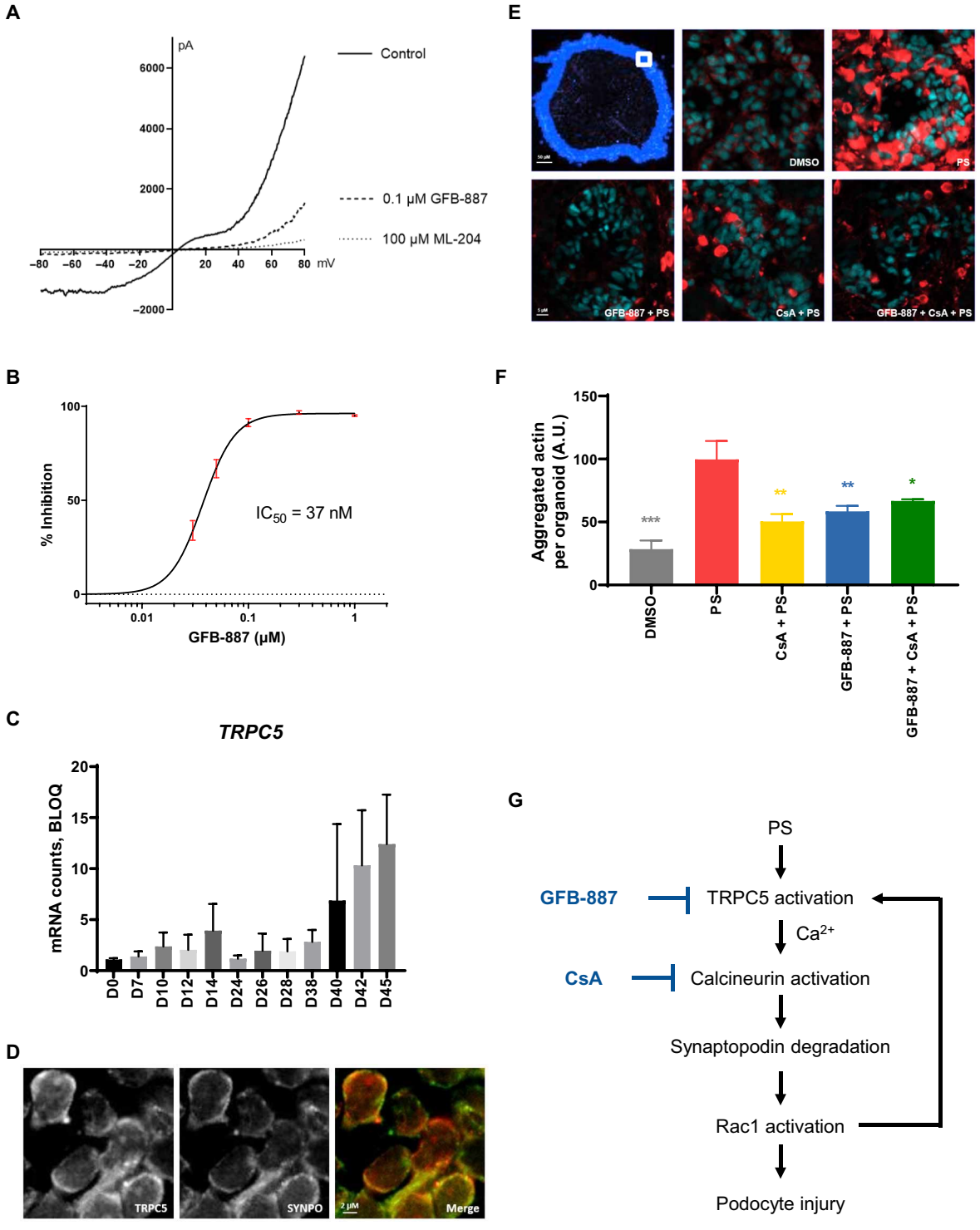

Fig. 2. In vitro drug evaluation in human kidney organoids. (**A**) Current-voltage relationship, 500-ms voltage ramp from −80 mV to +80 mV before/after GFB-887 (0.1 μM) or ML204 (100 μM). (**B**) Concentration-dependent inhibition of human TRPC5 after GFB-887 at +80 mV. Means ± SEM ($n = 3$ to 4 measurements per concentration). IC_{50}, median inhibitory concentration. (**C**) Up-regulation of human *TRPC5* mRNA expression during organoid differentiation in vitro. Error bars, SD. BLOQ, below limit of quantitation. (**D**) Double labeling of podocytes with synaptopodin (SYNPO, green) and TRPC5 (red). (**E**) CsA and GFB-887 protect podocytes from PS-induced injury, region of interest in blue. Inset: Scale of representative images for injury quantification (top left). Representative images of glomeruli for podocyte injury quantification in organoids treated with DMSO (vehicle), PS, PS + CsA, PS + GFB-887, or PS + CsA + GFB-887. Cyan, synaptopodin; red, phalloidin. (**F**) Quantification of PS-induced actin aggregation. GFB-887 and CsA are nonadditive. DMSO versus PS, $P < 0.0001$; PS + CsA versus PS, $P = 0.0021$; PS + GFB-887 versus PS, $P = 0.0087$; PS + CsA + GFB-887 versus PS, $P = 0.0397$. A.U., arbitrary units. Means ± SEM. (**G**) Mechanism of action of GFB-887. PS drives TRPC5 activity, which induces Ca^{2+}-mediated activation of calcineurin, promoting synaptopodin degradation and subsequent Rac1 activation. Rac1 promotes TRPC5 activity, establishing a vicious cycle that is blocked by GFB-887 or CsA.

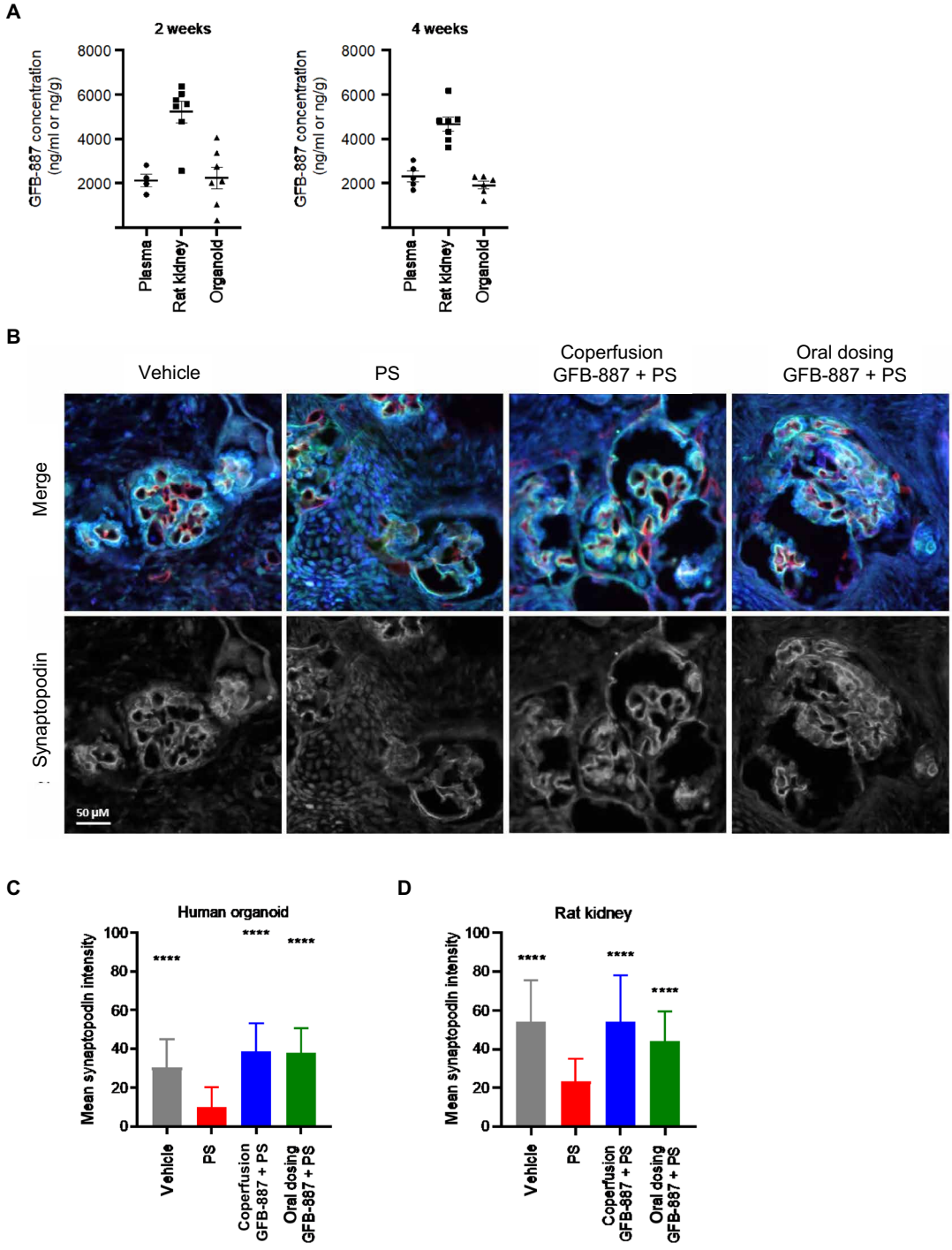

Fig. 3. PD studies in rats with transplanted human kidney organoids bolster confidence in GFB-887, an investigational new drug. (**A**) Organoids differentiated for 14 days in vitro were transplanted under the kidney capsule of athymic male rats and followed for 2 (left) or 4 (right) weeks before oral dosing with GFB-887 (10 mg/kg) for three consecutive days. Extracted organoid and kidney samples were normalized to sample weights, and the final drug values were calculated as nanograms per gram tissue; nanograms per milliliter refers to GFB-887 concentration per milliliter of plasma. Oral dosing of GFB-887 resulted in equivalent drug exposure in organoids and rat plasma, thereby showing that the organoids had functional connectivity to the host vasculature at 2 weeks after transplantation. Organoid GFB-887 levels did not further increase at 4 weeks after transplantation. Data show means ± SEM from at least four independent measurements. (**B**) Superresolution imaging reveals PS-induced loss of synaptopodin protein abundance in transplanted organoids, which was prevented by oral dosing of GFB-887; blue, nuclei; green, synaptopodin; red, RECA-1; HBSS, Hank's balanced salt solution vehicle control. (**C**) Quantification of PS-induced podocyte injury and protection by GFB-887 in transplanted organoids. (**D**) Quantification of PS-induced podocyte injury and protection by GFB-887 in endogenous rat kidney adjacent to transplanted organoids. For both (C) and (D), synaptopodin mean intensity in podocytes was quantified for HBSS vehicle, PS, coperfusion PS + GFB-887, or PS perfusion after oral dosing of GFB-887. Data show means ± SEM; for all treatment conditions versus PS, $P < 0.0001$; ordinary one-way analysis of variance (ANOVA). ****$P < 0.0001$.

for PD studies. We found that transplantation of organoids grown in vitro for 14 days and further grown in vivo for 4 weeks was best for organoid vascularization/perfusion (and podocyte differentiation).

The PD studies in rats carrying transplanted organoids provide unprecedented preclinical confidence in the human relevance of specific targets and compounds, marking a substantial advance that overcomes previous limitations of animal models. Specifically, our PD work showed that orally dosed GFB-887 protects human podocytes in transplanted organoids fed by a vasculature functionally connected to the rat host circulation, bolstering our confidence in this program as it advances in the clinic.

We confirmed published scRNA-seq data (*8*, *11*–*13*) and further validated them by NanoString analysis as an inexpensive tool for rapid organoid quality control in a drug discovery setting, affording close to real-time decision-making about whether to transplant organoids. Hence, NanoString organoid profiling offers a clear advantage compared to flow cytometry because of enhanced speed, ability to multiplex 200+ genes, reduced cost, and high reproducibility. Together, NanoString-based quality control proved to be essential for our ability to conduct in vivo PD studies in human tissue, a substantial innovation for biotechnology and drug discovery.

The podocyte protective effect of TRPC5 inhibition has been well documented before in cell culture studies and multiple animal models of proteinuria and FSGS using several structurally unrelated tool compounds, including ML204 (*27*, *34*), AC1903 (*31*), and GFB-8438 (*26*). The main purpose of the current study was the investigation of a novel compound, GFB-887, which is now tested in the clinic, and to establish the human relevance of TRPC5 inhibition. As the results in the translated organoids align well with the results in endogenous rat kidneys (Fig. 3), for the purposes of this study, the use of a single iPSC line turned out to be an excellent tool that was developed to drive this point. Notably, independent validation of the benefit of TRPC5 inhibition in organoids using the TRPC5-selective tool compound AC1903 (*31*) has recently been published (*40*). In the latter study, the inhibition of TRPC5 channels reversed the effects of puromycin aminonucleoside–induced injury in human podocytes and kidney organoids. These results further support the potential of this therapeutic strategy for patients (*40*).

The overarching key goal of our work was to establish the preclinical human disease relevance of a novel drug target, TRPC5, before its evaluation in patients with TRPC5/Rac1-mediated FSGS in a phase 2 clinical trial. Accordingly, a recently released interim analysis of phase 2 trial data of GFB-887 in FSGS provides the strongest validation to date for our preclinical experimental approach. These positive preliminary results of the ongoing phase 2 trial showed that patients treated with GFB-887 experienced a statistically significant and clinically meaningful 32% placebo-adjusted mean reduction in UPCR (urinary protein–to–creatinine ratio), a measure of proteinuria, at the end of 12 weeks of treatment ($P = 0.04$). Nine of the 10 evaluable GFB-887–treated patients (90%) experienced a reduction in UPCR; four of seven patients treated with placebo had an increase in UPCR (57%). In a subset of patients identified by a threshold reduction in a TRPC5-Rac1 pathway biomarker, urinary Rac1, at week 2 of treatment, patients treated with GFB-887 showed a 48% placebo-adjusted mean reduction in UPCR at the end of the 12-week treatment period (www.goldfinchbio.com/news-features/goldfinch-bio-announces-positive-preliminary-data-from-phase-2-clinical-trial-evaluating-gfb-887-as-a-precision-medicine-for-patients-with-focal-segmental-glomerular-sclerosis-fsgs/).

In conclusion, the most compelling aspect of our study is establishing the human relevance of an investigational new drug by performing PD studies in human kidney organoids transplanted into a rat host. More broadly, we show that PD studies using transplanted organoids are not only feasible but also meaningful and valuable for the assessment of the PD efficacy of a novel therapeutic candidate before going into expensive and time-consuming clinical trials. Our data support the idea that, if properly maintained and quality controlled, then human iPSC–derived organoid systems are likely to become an integral component of drug discovery programs in several tissues and organs, including, for example, the kidney, gut, eye, or brain. We are therefore at the dawn of a new era in drug discovery, where confidence in bringing novel drugs to the clinic may be derived, at least, in part, from establishing preclinical efficacy in transplanted human organoids.

MATERIALS AND METHODS

Maintenance of human iPSCs

In accordance with International Society for Stem Cell Research (ISSCR) guidelines, commercially approved and available human iPSCs (Gibco Episomal hiPSC line; part number: A18944; lot number: 1992258; passage: P35E8P15; Thermo Fisher Scientific, Waltham, MA) were maintained according to standard practice and cell culture on human embryonic stem cell (hESC)–qualified Matrigel (Corning, Corning, NY)–coated T25 flasks in mTeSR1 medium (STEMCELL Technologies, Vancouver, Canada) and passaged at 80 to 85% confluency using Gentle Cell Dissociation Reagent (STEMCELL Technologies). For evaluation of pluripotency by flow cytometry, iPSCs were dissociated with Accutase (STEMCELL Technologies), washed with Dulbecco's phosphate-buffered saline DPBS, fixed in 4% paraformaldelhyde (PFA) for 20 min at room temperature (RT), and rinsed with DPBS. The cells were incubated for 1 hour in a blocking buffer [DPBS containing 0.3% Triton X-100, 1% bovine serum albumin (BSA), and 5% donkey serum] and for 1 hour at 4°C with a combination of conjugated antibodies to surface proteins TRA-1-60 (STEMCELL Technologies, 60064PE) and TRA-1-81 (STEMCELL Technologies, 60065AZ), key transcription factors OCT3/4 (Santa Cruz Biotechnology, sc-5279) and NANOG (Thermo Fisher Scientific, 53-5761-80), and a negative surface marker SSEA1 (STEMCELL Technologies, 60060PE). Cells were washed with DPBS followed by data acquisition on a SONY SH800 flow cytometer. In accordance with ISSCR guidelines, commercially approved and available human iPSCs and derivations were banked after being assigned unique identifiers to deposits, characterized, tested for human pathogen, expanded, or maintained following quality assurance and quality control of all procedures in preparation for experimental application.

High-throughput kidney organoid generation

For the development of a reproducible scalable protocol, we introduced several key modifications to published protocols (*5*, *8*, *13*, *14*, *17*, *18*). We started by dispersing iPSCs reaching 80 to 85% confluency into single-cell suspensions using Accutase and seeding 275,000 cells per flask in hESC-qualified, Matrigel-coated T75 flasks with TeSR1 media and Y-27632 (Tocris 1254, Bristol, United Kingdom). On the next day, the medium was changed to STEMdiff APEL 2 (STEMCELL Technologies) supplemented with 10 μM CHIR99021 (Tocris 4423). After 48 hours, the medium was changed to STEMdiff APEL 2

supplemented with 8 μM CHIR99021. Subsequently, the medium was switched to STEMdiff APEL 2 with FGF9 (200 ng/ml; R&D Systems, Minneapolis, MN) and heparin (1 μg/ml; STEMCELL Technologies) and changed every other day. On D7, cells were passaged using Accutase and pelleted by centrifugation at 500,000 cells per pellet. The pellets were placed on Transwell plates, and STEMdiff APEL 2 supplemented with 5 μM CHIR99021 was added for 1 hour before changing to STEMdiff APEL 2 with FGF9 (200 ng/ml) and heparin (1 μg/ml). Medium was changed every other day for the next 4 days using STEMdiff APEL 2 containing FGF9 (200 ng/ml) and heparin (1 μg/ml). On D13, the medium was switched to STEMdiff APEL 2 with heparin (1 μg/ml). Thereafter, organoids were grown in STEMdiff APEL 2, and medium was changed every other day.

Organoid transplantation

Organoids differentiated in vitro as described above were transplanted into 3- to 4-week-old athymic male nude rats (Crl:NIH-Foxn1^{rnu}; Charles River Laboratories, Wilmington, MA) weighing approximately 100 g each, acclimated for at least 3 days in conventional cage setting with rodent diet 5053 and ad libitum water at Biomere Research test facility (Worcester, MA) in accordance with an approved Institutional Animal Care and Use Committee (IACUC) study protocol. Forty-five rats were divided into three experimental groups (D10, D12, and D14 differentiated) and anesthetized with ketamine/dexdomitor before surgery. The kidneys were exposed by an incision in the abdominal wall. After creating an incision in the kidney capsule, a small niche was created under the kidney capsule to host the organoids. Organoids grown for 10, 12, or 14 days in vitro were aspirated into the tip of an 18- to 24-gauge catheter (Instech Laboratories, Plymouth, PA) and placed into the niche, the abdominal wall and skin were closed, and the animals were allowed to recover and followed up with routine cage side observations for general health. To facilitate postsurgical recovery, an antibiotic (cephazolin) and an analgesic (buprenorphine sustained-release) were administered at the end of the procedure. At 2 or 4 weeks after transplantation, six to eight rats per experimental group were euthanized under CO_2, as per the IACUC-approved study protocol, and kidneys exposed by an incision in the abdominal wall and organoids ($n \geq 3$) were harvested for scRNA-seq and NanoString mRNA analysis as well as analysis of graft tissue vascularization. Organoid differentiation was also evaluated at the protein level by flow cytometry analysis of two podocyte surface proteins, nephrin (*41*) and podocalyxin (*42*). Cells from dissociated organoids were washed with DPBS, blocked in 1% mouse serum for 30 min at 4°C, incubated with anti-nephrin primary antibody (R&D Systems, AF4269) and allophycocyanin (APC)–conjugated anti-podocalyxin antibodies (R&D Systems, FAB1658A), and diluted in sorting buffer [Hanks' balanced salt solution (HBSS) containing 1% BSA and 0.035% $NaHCO_3$]. The cells were further incubated for 10 min in Alexa Fluor 488–conjugated donkey anti-sheep immunoglobulin G (IgG) (H+L) antibody (Thermo Fisher Scientific, A-11015), washed, and resuspended in sorting buffer. Unstained cells were used to establish background fluorescence. Data acquisition and analysis were performed on a SONY SH800 flow cytometer. Mean fluorescence in live cells was determined for each sample and is presented after subtraction of background fluorescence.

FACS flow cytometry

Cells were harvested, fixed, blocked, stained for FACS flow cytometry. For human iPSCs, D0 and D7 cell harvesting, mTeSR basal media was aspirated from the T25 flask, and cells were washed with 3 ml of 1× DPBS. DPBS (1×) was aspirated, and then 2 ml of undiluted Accutase, warmed to the RT, was added. Accutase was incubated for 5 min at 37°C. Five milliliters of cold 1× DPBS was added. A P1000 was used to gently pipet up and down to break up cell aggregates and remove cells from the flask. The cell suspension was transferred into a 15-ml conical tube and centrifuged for 4 min at 600*g* at RT. The supernatant was carefully aspirated. For fixation and blocking, cells were resuspended in 1 ml of 4% PFA and incubated for 20 min at RT. Cells were centrifuged for 4 min at 600*g* at RT, and then fixative was aspirated. The cell pellet was resuspended in 5 ml of 1× DPBS and then centrifuged again for 4 min at 600*g* at RT before the supernatant was removed. The cell pellet was resuspended in 2 ml of 1× DPBS and stored at 4°C until ready for immunostaining. Samples were stored at 4°C for 7 to 10 days maximally. To prepare for staining, the cell pellet was resuspended in 2 ml of blocking buffer and incubated for 30 min on ice. For staining, an aliquot of 150,000 to 250,000 cells was resuspended and placed in a separate Eppendorf tube and centrifuged for 4 min at 600*g*, the supernatant was removed, and the pellet was resuspended in 1× DPBS and stored on ice as a negative (nonstained) control. The rest of the cells were divided into three 1.5 Eppendorf tubes, one for each antibody set. Cells were then centrifuged for 4 min at 600*g*, and the supernatant was carefully aspirated and resuspended in 200 μl of primary antibodies cocktail. Anti-human TRA-1-60 (STEMCELL Technologies, 60064PE), anti-human TRA-1-81 (STEMCELL Technologies, 60060PE), anti-mouse SSEA-1 (CD15) (STEMCELL Technologies, 60060PE), anti–Oct-3/4 antibody (C-10) Alexa Fluor 647 (Santa Cruz Biotechnology, sc-5279 AF647), anti-NANOG monoclonal Alexa Fluor 488 (Thermo Fisher Scientific, 53-5761-80) antibodies were used at 1:100 dilution. After the cells were incubated for 30 to 60 min on ice with a foil covering to protect samples from the light, they were centrifuged for 4 min at 600*g* at RT. The supernatant was aspirated, resuspended in 1 ml of 1× DPBS, centrifuged for 4 min at 600*g*, and aspirated again until it, lastly, resuspended in a final volume of 250 μl of 1× DPBS. Data were acquired using the SONY SH800 cell sorter.

In vitro organoids D10 and above were rinsed with DPBS, collected into 1.5-ml conical tube containing 500 ml of TrypLE Select and incubated for 5 min at 37°C, passed three to four times through a 27-gauge needle, and incubated for 5 min at 37°C after adding an additional 500 ml of TrypLE Select. Organoids were dissociated into single-cell suspensions by passing three to four times through a 30-gauge needle, followed by centrifugation at 600*g* for 5 min. Supernatants were discarded, and cell pellets were resuspended in DPBS and filtered through a 40-mm cell strainer. Flow cytometry QC was conducted on all samples submitted for scRNA-seq. During blocking, dissociated cells were washed with 1× DPBS, centrifuged for 4 min at 600*g* at RT, then resuspended in normal mouse serum, and diluted in 1× DPBS (1:20) for 30 min on ice. The cell suspension was centrifuged for 4 min at 600*g* at RT, and the supernatant was removed. The cell pellet was resuspended in 2 ml of 1× DPBS and stored at 4°C until ready for immunostaining. During staining, an aliquot of 150,000 to 250,000 cells was placed in a separate Eppendorf tube and centrifuged for 4 min at 600*g* at 4°C, and then the supernatant was removed. These cells were then resuspended in 1× DPBS and left on ice as a negative (nonstained) control. The supernatant of cells from organoids was resuspended in SONY sorting buffer with diluted secondary antibodies. Anti-human nephrin

(R&D Systems, AF4269) and anti-human podocalyxin APC-conjugated (R&D Systems, FAB1658A) antibodies were used at 1:100 dilution. Cell samples were incubated with antibodies on ice for 30 min. Next, samples were centrifuged for 4 min at 600*g* at RT. The supernatant was aspirated and resuspended in a sorting buffer with diluted secondary antibodies. Donkey anti-sheep IgG (H+L) Alexa Fluor 488 (Invitrogen, A-11015) was used at 1:300. Cell samples incubated with antibodies were protected from the light with foil and incubated on ice for 30 min. Samples were then centrifuged for 4 min at 600*g*, the supernatant was aspirated, and cells were washed with 500 µl of sorting buffer. All cell pellets were resuspended in a final volume of 250 ml of 1× DPBS. Data were acquired using SONY SH800.

Gene expression analysis by scRNA-seq

Organoids were rinsed with DPBS, collected into a 1.5-ml conical tube containing 500 ml of TrypLE Select and incubated for 5 min at 37°C, passed three to four times through a 27-gauge needle, and incubated for 5 min at 37°C after adding an additional 500 µl of TrypLE Select. Organoids were dissociated into single-cell suspensions by passing three to four times through a 30-gauge needle, followed by centrifugation at 600*g* for 5 min. Supernatants were discarded, and cell pellets were resuspended in DPBS and filtered through a 40-µm cell strainer. Cell numbers were quantified on a Cellometer cell counter and adjusted to 1000 cells/µl in DPBS. The cells were placed on ice, transferred to the RNA-seq facility, introduced to droplet-based (10×) lysis and amplification, and sequenced on Illumina HiSeq 2500. For data obtained from in vitro organoids, sequences were aligned to human reference (GRCh38) and, for cells from transplanted organoids, to combined human and rat reference (Rnor 6.0) genomes. Demultiplexing, alignment, and estimation of cell-containing partitions and associated unique molecular identifiers were performed using Cell Ranger version 3.0.2. Replicates within time points were grouped, and a preliminary unbiased clustering analysis was performed on the top 50 principal components (PCs) of gene expression. Cells with high ribosomal gene content and low read count were considered poor-quality cells and excluded from further analyses. The remaining cells were filtered by the number of recovered genes and mitochondrial gene content. In total, high-quality libraries were generated for 348,223 cells that had passed QC. To infer cell type populations within each time point and condition, we used unbiased clustering of the top 50 PCs of residual gene expression after regressing out replicate, total gene count, mitochondrial gene content, and cell cycle score. We assigned cell type labels based on up-regulation of marker genes in the focal cluster as determined by a Wilcoxon rank sum test in Seurat 3.1 in R 3.6.1 (*43*). Divergences of cluster proportions and replicates were compared with JSD indices (*8*). The JSD is an entropy-based measurement of similarity between two samples bound between 0 (more similar) and 1 (more divergent). Cell type proportions were further tested across conditions using Dirichlet regression (*44*). For each comparison, the proportions of all other cell subsets were used as covariates. To compare podocyte maturation across time points and to data from fetal and adult human kidney samples (*22*, *45*), we performed a trajectory analysis using the top 1000 differentially expressed genes between the podocyte and nephron progenitor cell type clusters in Monocle 2 in R 3.6.1 (*46*). We reconstructed a trajectory of differentiation in pseudotime using the DDRTree algorithm implemented in Monocle 2 and compared pseudotime across conditions with a (two-sided) *t* test for comparing aggregated data by weeks and a post hoc Tukey testing of all pairwise comparisons of the individual time points (*47*). To compare the subpopulation of collecting duct-like cells to the distal tubular cells, we repeated the trajectory analysis as described above for these two subpopulations. Each measurement was taken from distinct samples (no repeat measurements on the same sample within a distinct analysis).

RNA extraction and quantification

Total RNA was extracted from organoids or dissociated organoid single-cell populations using the PureLink RNA Mini Kit (Life Technologies, Carlsbad, CA) following the manufacturer's instructions. Lysis buffer (200 ml) was used per organoid for homogenization at 12,000*g* for 2 min in a QIAshredder column (QIAGEN, Hilden, Germany) after lysis and before addition of 70% ethanol. Total RNA was eluted with 50 µl of ribonuclease (RNase)–free water and stored at −80°C until further use. Total RNA was quantified in a NanoDrop 2000c Spectrophotometer (Thermo Fisher Scientific).

NanoString gene expression analysis

A total of 100 ng of RNA from iPSCs, differentiated cells, organoids, human normal fetal kidney (Takara, 636584-1412044) or adult kidney (Takara, 636529-1807151) in 5 µl of RNase-free water was subjected to NanoString nCounter Elements workflow, according to the nCounter Elements XT Assay User Manual (NanoString Technologies, Seattle, WA). mRNA expression of 228 genes was assessed using nSolver 4.0 software (NanoString Technologies). The gene panel (table S1) included pluripotency markers (e.g., *NANOG*, *POU5F1*, and *SOX2*), kidney-specific markers (early development: *SIX2*, *LHX1*, and *OSR1*; mature podocytes: *SYNPO*, *PODXL*, *NPHS1*, and *NPHS2*), and markers of off-target cell types (e.g., *CRABP1*, *HES6*, and *PMEL*). Gene expression levels of 222 genes were normalized using six reference genes (*ABCF1*, *GUSB*, *HPRT1*, *LDHA*, *POLR1B*, and *RPLP0*), which were included in the gene panel (total of 228). Heatmaps were generated using the Python Seaborn package and displayed as hierarchical clustering (rows) of *z* score transformed expression values. For comparison of NanoString data to scRNA-seq data, normalized, log-transformed counts for the 222 genes on the NanoString panel were extracted and averaged across each cluster (Seurat function "AverageExpression"). Eighteen genes that were not detected at any developmental stage were dropped. Heatmaps were generated using R package "pheatmap." Row *z*-scaled gene expression matrix was clustered (hierarchically) using Euclidean distance metric.

Electrophysiology

Manual patch-clamp electrophysiology was performed in the whole-cell configuration in HEK293 cells stably overexpressing human TRPC5 according to published protocols (*27*), using previously reported external and internal solutions (*27*). Once in the whole-cell configuration, cells were held at 0 mV, and TRPC5 current was measured by an initial step to −80 mV held for 50 ms, followed by a ramp protocol from −80 mV to +80 mV at a rate of 1 mV/ms, and then a step at +80 mV for 50 ms before returning to the holding potential. The voltage protocol was repeated at a frequency of 1 Hz. Mean inward and outward currents were determined at −80 mV and +80 mV, respectively. GFB-887 and ML204 (*27*) were delivered to cells diluted at final concentration in external buffer through a gravity perfusion system (*27*).

Compound treatment of organoids in vitro

D24 to D28 in vitro organoids were used for CsA or GFB-887 compound treatment. CsA was diluted from a 20 mM stock in dimethyl sulfoxide (DMSO) to final concentrations of 20, 2, 0.2, or 0.02 μM in STEMdiff APEL 2, and GFB-887 was diluted from a 10 mM stock in DMSO to final concentrations of 10, 1, 0.1, or 0.01 μM in STEMdiff APEL 2. Compound stability in solution was analyzed using Waters ACQUITY ultra performance liquid chromatography. One milliliter of GFB-887–containing medium was added to the apical side of the Transwell insert, and 2 ml of GFB-887–containing medium was added to the basolateral side of the Transwell insert. Organoids were pretreated with compounds separately or in combination for 1 hour before exposure to PS at 300 μg/ml (Sigma-Aldrich) for an additional 1, 6, or 24 hours.

Immunofluorescence microscopy

Organoids grown in vitro or transplanted organoids connected to adjacent endogenous rat kidneys were rinsed with DPBS and fixed with 4% PFA at RT for 30 min, washed twice with DPBS for 5 min at RT, and incubated in 30% sucrose at 4°C for 2 to 3 days. After freezing the samples in optimal cutting temperature (VWR, Radnor, PA), sections were cut on a Leica CM1950 cryostat, collected at a thickness of 10 μm, placed on glass slides, treated with 0.1% Triton X-100, and blocked in 10% donkey or goat serum. After incubation with primary antibodies overnight at 4°C, sections were washed with DPBS and incubated with secondary antibodies for 1 hour at RT. Primary antibodies included the following: CD31/PECAM1 (Bethyl Laboratories, IHC-00055), RECA-1 (Bio-Rad, MCA970GA), synaptopodin (Progen, GP94-N), E-cadherin (R&D Systems, AF648), TRPC5 [University of California Davis/National Institutes of Health (NIH) NeuroMab Facility, 75-104], and TRPC5 (Alomone Labs, ACC-020). Secondary antibodies included the following: Alexa Fluor 647 donkey anti-rat, Alexa Fluor 555 donkey anti-mouse, Alexa Fluor 555 donkey anti-rabbit, Alexa Fluor 488 donkey anti-rabbit, Alexa Fluor 488 donkey anti-goat (Thermo Fisher Scientific), Alexa Fluor 647 donkey anti-guinea pig (the Jackson Laboratory), Alexa Fluor 405 donkey anti-goat (Abcam), and Alexa Fluor 750 donkey anti-goat (Abcam). They were used at 1:300 for 1 hour at RT, and Hoechst 33342 was used at 1:10,000 and phalloidin at 1:1000 for 30 min at RT. Fluorescence microscopy images were captured on a digital Axio Scan.Z1 Slide Scanner (Carl Zeiss, White Plains, NY) (objective Plan-Apochromat 20×/0.8; Hamamatsu Camera, Transmitted light detector T-PMT, filter sets 90 HE LED and 110 HE LED, Axio Scan.Z1) or a superresolution confocal LSM 880 Airyscan microscope [Carl Zeiss Plan-Apochromat objective 20×/0.8 WD = 0.55 M27, Axio Observer Z1 for LSM880, Transmitted light detector T-PMT, filter sets 49 4′,6-diamidino-2-phenylindole (DAPI) EXG365 S free, 43 Cy3 shift free, and 38 HE green fluorescent protein shift free]. Zen5 software powered by Arivis was used for image acquisition and processing.

Quantification of podocyte injury in human kidney organoids in vitro

For semi-automated image analysis with Amira for Cell Biology imaging software, the 4′,6-diamidino-2-phenylindole (DAPI) channel was used to identify cells and to create an organoid mask, the phalloidin channel was used to identify penetration depth of PS injury and to create a mask for region of injury quantitation, and the synaptopodin channel was used to identify injured podocytes. Using overlays of the DAPI channel mask to limit detection to organoid tissue on a slide, the phalloidin channel mask to limit detection to the region of injury, and the synaptopodin channel masks to limit detection to the regions containing podocytes, we used Amira to provide quantitative readouts of average phalloidin intensity over podocyte surface areas. GraphPad Prism 8.0.1 was used to graph the quantitative readout of aggregated actin and perform ordinary one-way analysis of variance (ANOVA) for multiple comparisons.

PK studies in rats with transplanted organoids

For PK studies, 5- to 6-week-old athymic male nude rats with D14 transplanted organoids were used. Animals were randomly divided into three experimental groups (vehicle, GFB-887 acute, and GFB-887 chronic) with at least four animals per group. GFB-887 (10 mg/kg) formulated in vehicle solution [Solutol HS-15 (Sigma-Aldrich), vitamin E-TPGS (PMC Isochem, France), and polyethylene glycol 300 (Sigma-Aldrich)] or vehicle alone was dosed orally once per day for three consecutive days. For direct administration of GFB-887 or vehicle into the renal artery, an incision was made in the abdominal wall of rats euthanized with CO_2 according to an approved IACUC protocol, followed by exposing and clamping the supra- and infrarenal abdominal aorta. A small incision was made into the inferior vena cava to allow drainage of the perfusion solution. First, the rat kidney/human organoid pairs were flushed with HBSS at 9 ml/min for 5 min through a fine catheter (Exel, Santa Ana, CA) inserted into the clamped abdominal aorta, followed by further perfusion for 15 min with 3 μM GFB-887 and 0.3% DMSO in HBSS or 0.3% DMSO in HBSS (serving as control). At the end of the perfusion, the organoids and host kidneys were excised together ($n \geq 3$), rinsed with ice-cold DPBS, snap-frozen in liquid nitrogen, and stored at −80°C until further use. Blood samples (100 to 200 μl) were drawn 4 hours after oral dosing on D1 and D2 and at 30 min, 1, 2, and 4 hours after dosing on D3 and collected on ice in K2-EDTA (Thermo Fisher Scientific) containing microcentrifuged tubes. Within 30 min after collection, the blood samples were processed to plasma by centrifugation at 10,000 rpm at 4°C. Plasma samples were snap-frozen in liquid nitrogen and stored at −80°C until further use. GFB-887 concentrations in organoids, rat kidneys, and rat plasma samples were measured by liquid chromatography (LC)–mass spectrometry at RMI Laboratories (North Wales, PA). Organoid and kidney sample processing involved homogenization with 0.5-mm zirconium beads for 45 s at 4000 cycles/min in 500 to 1000 μl of 50:50 acetonitrile/water mixture containing internal standard (0.1 μg/ml) and 0.1% formic acid (FA). Supernatants were spun at 13,000 rpm for 5 min, and 100 μl of the supernatant was mixed with 100 μl of 0.1% FA solution before LC–tandem mass spectrometry (MS/MS) analysis. Full-scan LC-MS/MS data were analyzed with QuanLynx software for internal standards and GFB-887. Data were quantified using a matrix-specific six-point calibration curve spiked with GFB-887. The initial values from plasma, organoid, and kidney samples were reported as nanograms per milliliter by RMI Laboratories who conducted the measurements. Using a density of 1 for mass to volume conversion, the organoid and kidney samples were then normalized to their respective sample weights, and the final drug values in the tissue samples were reported as nanograms per gram tissue.

PD studies in rats with transplanted organoids

PS-induced podocyte foot process effacement (*32*, *33*) was assessed in rats with D14 kidney organoids grown in vivo for 4 weeks. After

clamping the renal artery and excision of one organoid/kidney pair for PK studies, vascular perfusion of the contralateral kidney/organoid pair at a flow rate of 9 ml/min was done as follows: (i) vehicle control group (n = 2): 5 min of HBSS, 30 min of 0.3% DMSO in HBSS, 5 min of HBSS, and 5 min of fixative (4% PFA in DPBS); (ii) PS group (n = 2): 5 min of HBSS, 15 min of 0.3% DMSO in HBSS, 15 min of PS (2 mg/ml) in 0.3% DMSO, 5 min of HBSS, and 5 min of fixative; (iii) PS + oral GFB-887 dosing group (n = 3): 5 min of HBSS, 15 min of PS (2 mg/ml) and 0.3% DMSO in HBSS, 5 min of HBSS washout, and 5 min of fixative; (iv) renal artery GFB-887 dosing group (n = 3): 5 min of HBSS, 15 min of PS (2 mg/ml) and 3 μM GFB-887, 0.3% DMSO in HBSS, 5 min of HBSS, and 5 min of fixative. After fixation, organoids and host kidneys were excised together, rinsed with ice-cold DPBS, trimmed and immersion-fixed in 4% PFA for 24 to 48 hours at 4°C, transferred to 30% sucrose, and stored at 4°C until further use. Host rat kidney and organoids were imaged together on the same slide to ensure uniform and comparative images for quantitation.

Quantification of podocyte injury in transplanted organoids and adjacent rat kidney

D14 organoids transplanted for 4 weeks and the adjacent endogenous rat kidneys were processed for immunofluorescence whole scan image acquisition of organoid and adjacent rat tissue, and 10 to 12 50× zoomed images were randomly acquired (pixel size, 0.33 × 0.33 × 0.5 XYZ μM) for each condition and quantified using OMERO 5.6 viewer (*48*) and Fiji/ImageJ 1.52 g (open-source NIH imaging software). Staining for nephrin and synaptopodin was used to identify podocytes in glomeruli of transplanted organoids and endogenous rat kidneys. Using overlays of the nephrin channel mask to limit detection to podocytes, Fiji/ImageJ was used for quantification of synaptopodin abundance and phalloidin average intensity over the surface area within nephrin-positive masked areas ±SEM for the following number of randomly acquired glomerular structures for each condition: (A) organoids: (i) vehicle control group (n = 56), (ii) PS group (n = 59), (iii) PS + oral GFB-887 dosing group (n = 89), and (iv) renal artery GFB-887 dosing group (n = 74); (B) rat kidney: (i) vehicle control group (n = 70), (ii) PS group (n = 79), (iii) PS + oral GFB-887 dosing group (n = 127), and (iv) renal artery GFB-887 dosing group (n = 147). GraphPad Prism was used to graph the quantitative readout of synaptopodin intensity and perform ordinary one-way ANOVA followed by Dunnett's multiple comparisons test.

SUPPLEMENTARY MATERIALS

Supplementary material for this article is available at https://science.org/doi/10.1126/sciadv.abj5633

View/request a protocol for this paper from *Bio-protocol*.

REFERENCES AND NOTES

1. J. K. Inrig, R. M. Califf, A. Tasneem, R. K. Vegunta, C. Molina, J. W. Stanifer, K. Chiswell, U. D. Patel, The landscape of clinical trials in nephrology: A systematic review of Clinicaltrials.gov. *Am. J. Kidney Dis.* **63**, 771–780 (2014).
2. K. J. Jager, C. Kovesdy, R. Langham, M. Rosenberg, V. Jha, C. Zoccali, A single number for advocacy and communication-worldwide more than 850 million individuals have kidney diseases. *Kidney Int.* **96**, 1048–1050 (2019).
3. T. Takahashi, Organoids for drug discovery and personalized medicine. *Annu. Rev. Pharmacol. Toxicol.* **59**, 447–462 (2019).
4. M. Dvela-Levitt, M. Kost-Alimova, M. Emani, E. Kohnert, R. Thompson, E. H. Sidhom, A. Rivadeneira, N. Sahakian, J. Roignot, G. Papagregoriou, M. S. Montesinos, A. R. Clark, D. McKinney, J. Gutierrez, M. Roth, L. Ronco, E. Elonga, T. A. Carter, A. Gnirke, M. Melanson, K. Hartland, N. Wieder, J. C. Hsu, C. Deltas, R. Hughey, A. J. Bleyer, S. Kmoch, M. Zivna, V. Baresova, S. Kota, J. Schlondorff, M. Heiman, S. L. Alper, F. Wagner, A. Weins, T. R. Golub, E. S. Lander, A. Greka, Small molecule targets TMED9 and promotes lysosomal degradation to reverse proteinopathy. *Cell* **178**, 521–535.e23 (2019).
5. R. Morizane, A. Q. Lam, B. S. Freedman, S. Kishi, M. T. Valerius, J. V. Bonventre, Nephron organoids derived from human pluripotent stem cells model kidney development and injury. *Nat. Biotechnol.* **33**, 1193–1200 (2015).
6. A. Taguchi, R. Nishinakamura, Higher-order kidney organogenesis from pluripotent stem cells. *Cell Stem Cell* **21**, 730–746.e6 (2017).
7. S. Sharmin, A. Taguchi, Y. Kaku, Y. Yoshimura, T. Ohmori, T. Sakuma, M. Mukoyama, T. Yamamoto, H. Kurihara, R. Nishinakamura, Human induced pluripotent stem cell-derived podocytes mature into vascularized glomeruli upon experimental transplantation. *J. Am. Soc. Nephrol.* **27**, 1778–1791 (2016).
8. A. Subramanian, E. H. Sidhom, M. Emani, K. Vernon, N. Sahakian, Y. Zhou, M. Kost-Alimova, M. Slyper, J. Waldman, D. Dionne, L. T. Nguyen, A. Weins, J. L. Marshall, O. Rosenblatt-Rosen, A. Regev, A. Greka, Single cell census of human kidney organoids shows reproducibility and diminished off-target cells after transplantation. *Nat. Commun.* **10**, 5462 (2019).
9. C. W. van den Berg, L. Ritsma, M. C. Avramut, L. E. Wiersma, B. M. van den Berg, D. G. Leuning, E. Lievers, M. Koning, J. M. Vanslambrouck, A. J. Koster, S. E. Howden, M. Takasato, M. H. Little, T. J. Rabelink, Renal subcapsular transplantation of PSC-derived kidney organoids induces neo-vasculogenesis and significant glomerular and tubular maturation in vivo. *Stem Cell Rep.* **10**, 751–765 (2018).
10. A. J. Majmundar, F. Buerger, T. A. Forbes, V. Klambt, R. Schneider, K. Deutsch, T. M. Kitzler, S. E. Howden, M. Scurr, K. S. Tan, M. Krzeminski, E. Widmeier, D. A. Braun, E. Lai, I. Ullah, A. Amar, A. Kolb, K. Eddy, C. H. Chen, D. Salmanullah, R. Dai, M. Nakayama, I. Ottlewski, C. M. Kolvenbach, A. C. Onuchic-Whitford, Y. Mao, N. Mann, M. M. Nabhan, S. Rosen, J. D. Forman-Kay, N. A. Soliman, A. Heilos, R. Kain, C. Aufricht, S. Mane, R. P. Lifton, S. Shril, M. H. Little, F. Hildebrandt, Recessive *NOS1AP* variants impair actin remodeling and cause glomerulopathy in humans and mice. *Sci. Adv.* **7**, eabe1386 (2021).
11. T. Tran, N. O. Lindstrom, A. Ransick, G. De Sena Brandine, Q. Guo, A. D. Kim, B. Der, J. Peti-Peterdi, A. D. Smith, M. Thornton, B. Grubbs, J. A. McMahon, A. P. McMahon, In vivo developmental trajectories of human podocyte inform in vitro differentiation of pluripotent stem cell-derived podocytes. *Dev. Cell* **50**, 102–116.e6 (2019).
12. L. J. Hale, S. E. Howden, B. Phipson, A. Lonsdale, P. X. Er, I. Ghobrial, S. Hosawi, S. Wilson, K. T. Lawlor, S. Khan, A. Oshlack, C. Quinlan, R. Lennon, M. H. Little, 3D organoid-derived human glomeruli for personalised podocyte disease modelling and drug screening. *Nat. Commun.* **9**, 5167 (2018).
13. J. L. Harder, R. Menon, E. A. Otto, J. Zhou, S. Eddy, N. L. Wys, C. O'Connor, J. Luo, V. Nair, C. Cebrian, J. R. Spence, M. Bitzer, O. G. Troyanskaya, J. B. Hodgin, R. C. Wiggins, B. S. Freedman, M. Kretzler; European Renal cDNA Bank (ERCB); Nephrotic Syndrome Study Network (NEPTUNE), Organoid single cell profiling identifies a transcriptional signature of glomerular disease. *JCI Insight* **4**, e122697 (2019).
14. M. Takasato, P. X. Er, H. S. Chiu, M. H. Little, Generation of kidney organoids from human pluripotent stem cells. *Nat. Protoc.* **11**, 1681–1692 (2016).
15. A. Greka, P. Mundel, Cell biology and pathology of podocytes. *Annu. Rev. Physiol.* **74**, 299–323 (2012).
16. V. D. D'Agati, F. J. Kaskel, R. J. Falk, Focal segmental glomerulosclerosis. *N. Engl. J. Med.* **365**, 2398–2411 (2011).
17. M. Takasato, P. X. Er, H. S. Chiu, B. Maier, G. J. Baillie, C. Ferguson, R. G. Parton, E. J. Wolvetang, M. S. Roost, S. M. Lopes, M. H. Little, Kidney organoids from human iPS cells contain multiple lineages and model human nephrogenesis. *Nature* **536**, 238 (2016).
18. M. Takasato, M. H. Little, Making a kidney organoid using the directed differentiation of human pluripotent stem cells. *Methods Mol. Biol.* **1597**, 195–206 (2017).
19. M. S. Kowalczyk, I. Tirosh, D. Heckl, T. N. Rao, A. Dixit, B. J. Haas, R. K. Schneider, A. J. Wagers, B. L. Ebert, A. Regev, Single-cell RNA-seq reveals changes in cell cycle and differentiation programs upon aging of hematopoietic stem cells. *Genome Res.* **25**, 1860–1872 (2015).
20. J. H. Low, P. Li, E. G. Y. Chew, B. Zhou, K. Suzuki, T. Zhang, M. M. Lian, M. Liu, E. Aizawa, C. Rodriguez Esteban, K. S. M. Yong, Q. Chen, J. M. Campistol, M. Fang, C. C. Khor, J. N. Foo, J. C. Izpisua Belmonte, Y. Xia, Generation of human PSC-derived kidney organoids with patterned nephron segments and a de novo vascular network. *Cell Stem Cell* **25**, 373–387.e9 (2019).
21. C. E. Gillies, R. Putler, R. Menon, E. Otto, K. Yasutake, V. Nair, P. Hoover, D. Lieb, S. Li, S. Eddy, D. Fermin, M. T. McNulty; Nephrotic Syndrome Study Network (NEPTUNE), N. Hacohen, K. Kiryluk, M. Kretzler, X. Wen, M. G. Sampson, An eQTL landscape of kidney tissue in human nephrotic syndrome. *Am. J. Hum. Genet.* **103**, 232–244 (2018).
22. R. Menon, E. A. Otto, A. Kokoruda, J. Zhou, Z. Zhang, E. Yoon, Y. C. Chen, O. Troyanskaya, J. R. Spence, M. Kretzler, C. Cebrian, Single-cell analysis of progenitor cell dynamics and lineage specification in the human fetal kidney. *Development* **145**, dev164038 (2018).

23. H. Wu, K. Uchimura, E. L. Donnelly, Y. Kirita, S. A. Morris, B. D. Humphreys, Comparative analysis and refinement of human PSC-derived kidney organoid differentiation with single-cell transcriptomics. *Cell Stem Cell* **23**, 869–881.e8 (2018).
24. A. Subramanian, E. H. Sidhom, M. Emani, N. Sahakian, K. Vernon, Y. Zhou, M. Kost-Alimova, A. Weins, M. Slyper, J. Waldman, D. Dionne, L. T. Nguyen, J. Marshall, O. Rosenblatt-Rosen, A. Regev, A. Greka, Kidney organoid reproducibility across multiple human iPSC lines and diminished off target cells after transplantation revealed by single cell transcriptomics. *bioRxiv* , 516807 (2019).
25. P. W. Mathieson, Proteinuria and immunity—An overstated relationship? *N. Engl. J. Med.* **359**, 2492–2494 (2008).
26. M. Yu, M. W. Ledeboer, M. Daniels, G. Malojcic, T. T. Tibbitts, M. Coeffet-Le Gal, X. R. Pan-Zhou, A. Westerling-Bui, M. Beconi, J. F. Reilly, P. Mundel, J. C. Harmange, Discovery of a potent and selective TRPC5 inhibitor, efficacious in a focal segmental glomerulosclerosis model. *ACS Med. Chem. Lett.* **10**, 1579–1585 (2019).
27. D. Tian, S. M. Jacobo, D. Billing, A. Rozkalne, S. D. Gage, T. Anagnostou, H. Pavenstadt, H. H. Hsu, J. Schlondorff, A. Ramos, A. Greka, Antagonistic regulation of actin dynamics and cell motility by TRPC5 and TRPC6 channels. *Sci. Signal.* **3**, ra77 (2010).
28. P. Mundel, H. W. Heid, T. M. Mundel, M. Kruger, J. Reiser, W. Kriz, Synaptopodin: An actin-associated protein in telencephalic dendrites and renal podocytes. *J. Cell Biol.* **139**, 193–204 (1997).
29. P. Mundel, P. Gilbert, W. Kriz, Podocytes in glomerulus of rat kidney express a characteristic 44 KD protein. *J. Histochem. Cytochem.* **39**, 1047–1056 (1991).
30. V. D'Agati, The many masks of focal segmental glomerulosclerosis. *Kidney Int.* **46**, 1223–1241 (1994).
31. Y. Zhou, P. Castonguay, E. H. Sidhom, A. R. Clark, M. Dvela-Levitt, S. Kim, J. Sieber, N. Wieder, J. Y. Jung, S. Andreeva, J. Reichardt, F. Dubois, S. C. Hoffmann, J. M. Basgen, M. S. Montesinos, A. Weins, A. C. Johnson, E. S. Lander, M. R. Garrett, C. R. Hopkins, A. Greka, A small-molecule inhibitor of TRPC5 ion channels suppresses progressive kidney disease in animal models. *Science* **358**, 1332–1336 (2017).
32. D. Kerjaschki, Polycation-induced dislocation of slit diaphragms and formation of cell junctions in rat kidney glomeruli. The effects of low temperature, divalent cations, colchicine, and cytochalasin B. *Lab. Invest.* **39**, 430–440 (1978).
33. M. W. Seiler, M. A. Venkatachalam, R. S. Cotran, Glomerular epithelium: Structural alterations induced by polycations. *Science* **189**, 390–393 (1975).
34. T. Schaldecker, S. Kim, C. Tarabanis, D. Tian, S. Hakroush, P. Castonguay, W. Ahn, H. Wallentin, H. Heid, C. R. Hopkins, C. W. Lindsley, A. Riccio, L. Buvall, A. Weins, A. Greka, Inhibition of the TRPC5 ion channel protects the kidney filter. *J. Clin. Invest.* **123**, 5298–5309 (2013).
35. L. Buvall, H. Wallentin, J. Sieber, S. Andreeva, H. Y. Choi, P. Mundel, A. Greka, Synaptopodin is a coincidence detector of tyrosine versus serine/threonine phosphorylation for the modulation of rho protein crosstalk in podocytes. *J. Am. Soc. Nephrol.* **28**, 837–851 (2017).
36. C. Faul, M. Donnelly, S. Merscher-Gomez, Y. H. Chang, S. Franz, J. Delfgaauw, J. M. Chang, H. Y. Choi, K. N. Campbell, K. Kim, J. Reiser, P. Mundel, The actin cytoskeleton of kidney podocytes is a direct target of the antiproteinuric effect of cyclosporine A. *Nat. Med.* **14**, 931–938 (2008).
37. K. Asanuma, K. Kim, J. Oh, L. Giardino, S. Chabanis, C. Faul, J. Reiser, P. Mundel, Synaptopodin regulates the actin-bundling activity of α-actinin in an isoform-specific manner. *J. Clin. Invest.* **115**, 1188–1198 (2005).
38. L. Ning, H. Y. Suleiman, J. H. Miner, Synaptopodin is dispensable for normal podocyte homeostasis but is protective in the context of acute podocyte injury. *J. Am. Soc. Nephrol.* **31**, 2815–2832 (2020).
39. H. Y. Suleiman, R. Roth, S. Jain, J. E. Heuser, A. S. Shaw, J. H. Miner, Injury-induced actin cytoskeleton reorganization in podocytes revealed by super-resolution microscopy. *JCI Insight* **2**, e94137 (2017).
40. Y. Zhou, C. Kim, J. L. B. Pablo, F. Zhang, J. Y. Jung, L. Xiao, S. Bazua-Valenti, M. Emani, C. R. Hopkins, A. Weins, A. Greka, TRPC5 channel inhibition protects podocytes in puromycin-aminonucleoside induced nephrosis models. *Front. Med.* **8**, 721865 (2021).
41. M. Kestila, U. Lenkkeri, M. Mannikko, J. Lamerdin, P. McCready, H. Putaala, V. Ruotsalainen, T. Morita, M. Nissinen, R. Herva, C. E. Kashtan, L. Peltonen, C. Holmberg, A. Olsen, K. Tryggvason, Positionally cloned gene for a novel glomerular protein—Nephrin—Is mutated in congenital nephrotic syndrome. *Mol. Cell* **1**, 575–582 (1998).
42. D. Kerjaschki, D. J. Sharkey, M. G. Farquhar, Identification and characterization of podocalyxin—The major sialoprotein of the renal glomerular epithelial cell. *J. Cell Biol.* **98**, 1591–1596 (1984).
43. A. Butler, P. Hoffman, P. Smibert, E. Papalexi, R. Satija, Integrating single-cell transcriptomic data across different conditions, technologies, and species. *Nat. Biotechnol.* **36**, 411–420 (2018).
44. C. S. Smillie, M. Biton, J. Ordovas-Montanes, K. M. Sullivan, G. Burgin, D. B. Graham, R. H. Herbst, N. Rogel, M. Slyper, J. Waldman, M. Sud, E. Andrews, G. Velonias, A. L. Haber, K. Jagadeesh, S. Vickovic, J. Yao, C. Stevens, D. Dionne, L. T. Nguyen, A. C. Villani, M. Hofree, E. A. Creasey, H. Huang, O. Rozenblatt-Rosen, J. J. Garber, H. Khalili, A. N. Desch, M. J. Daly, A. N. Ananthakrishnan, A. K. Shalek, R. J. Xavier, A. Regev, Intra- and inter-cellular rewiring of the human colon during ulcerative colitis. *Cell* **178**, 714–730.e22 (2019).
45. H. Wu, A. F. Malone, E. L. Donnelly, Y. Kirita, K. Uchimura, S. M. Ramakrishnan, J. P. Gaut, B. D. Humphreys, Single-cell transcriptomics of a human kidney allograft biopsy specimen defines a diverse inflammatory response. *J. Am. Soc. Nephrol.* **29**, 2069–2080 (2018).
46. X. Qiu, A. Hill, J. Packer, D. Lin, Y. A. Ma, C. Trapnell, Single-cell mRNA quantification and differential analysis with Census. *Nat. Methods* **14**, 309–315 (2017).
47. J. W. Tukey, Comparing individual means in the analysis of variance. *Biometrics* **5**, 99–114 (1949).
48. J. M. Burel, S. Besson, C. Blackburn, M. Carroll, R. K. Ferguson, H. Flynn, K. Gillen, R. Leigh, S. Li, D. Lindner, M. Linkert, W. J. Moore, B. Ramalingam, E. Rozbicki, A. Tarkowska, P. Walczysko, C. Allan, J. Moore, J. R. Swedlow, Publishing and sharing multi-dimensional image data with OMERO. *Mamm. Genome* **26**, 441–447 (2015).

Acknowledgments: We thank E. Murray for technical support; A. Tebbe for computational support in setting up the computational infrastructure, installing crucial analysis packages, and making code and datasets available in the public domain; the Whitehead Institute Genome Technology Core for scRNA-seq library preparation and sequencing; the Harvard Center for Biological Imaging (HCBI) for help with imaging; B. Fish and the Biomere team for conducting the organoid transplantation studies; and ICAGEN for conducting the electrophysiology studies. **Funding:** No funding was received in support of this research.
Author contributions: A.D.W.-B., E.M.F., T.W.S., X.-R.P.-Z., J.-C.H., J.F.R., and P.M. designed the studies and interpreted the results. A.D.W.-B. performed experiments and coordinated data analysis. S.V., A.B.F., S.K., H.H., G.M.C., M.Y., M.D., G.M., M.W.L., and M.E. performed, supported, and analyzed additional experiments. M.D.R., E.M.F., W.Z., and T.W.S. performed computational analysis of scRNA-seq and NanoString data. T.T.T. assisted with data analysis. A.D.W.-B., E.M.F., T.W.S., and P.M. wrote the manuscript. P.M. supervised the project. All authors have read and approved the manuscript. **Competing interests:** P.M. is a co-founder and equity holder of Goldfinch Bio. A.D.W.-B., T.W.S., S.V., A.B.F., H.H., G.M.C., W.Z., M.Y., M.D., G.M., X.-R.P.-Z., M.W.L., J.-C.H., and T.T.T. are equity holders of Goldfinch Bio. The authors declare that they have no other competing interests. **Data and materials availability:** All data needed to evaluate the conclusions in the paper are present in the paper and/or the Supplementary Materials. The scRNA-seq datasets (raw data and count matrices) generated during this study are available at GEO (GSE165104). All analysis code has been deposited in the following GitHub repository and to Zenodo: https://github.com/goldfinchbio/organoid-paper and https://zenodo.org/record/6308367#.YmFbtPPMIeY. Interim analysis of phase 2 trial data of GFB-887 in FSGS is provided in this press release: www.goldfinchbio.com/news-features/goldfinch-bio-announces-positive-preliminary-data-from-phase-2-clinical-trial-evaluating-gfb-887-as-a-precision-medicine-for-patients-with-focal-segmental-glomerular-sclerosis-fsgs/.

Submitted 20 May 2021
Accepted 19 May 2022
Published 6 July 2022
10.1126/sciadv.abj5633